Factor Graphs for Support Identification in Compressive Sensing Aided WSNs

Jue Chen, Tsang-Yi Wang, *Member, IEEE*, Jwo-Yuh Wu, *Member, IEEE*, Chih-Peng Li, *Fellow, IEEE*, Soon Xin Ng, *Senior Member, IEEE*, Robert G. Maunder, *Senior Member, IEEE* and Lajos Hanzo, *Fellow, IEEE*

***Abstract*—A new support identification technique based on factor graphs and belief propagation is proposed for Compressive Sensing (CS) aided Wireless Sensor Networks (WSNs), which reliably estimates the locations of non-zero entries in a sparse signal through an iterative process. Our factor graph based approach achieves a support identification error rate of 10% at an Signal to Noise Ratio (SNR) that is 6 dB lower than that required by the state-of-the-art relative frequency based support identification approach, as well as by the Orthogonal Matching Pursuit (OMP) algorithm. We also demonstrate that our support identification technique is capable of mitigating the signal reconstruction noise by as much as 4 dB upon pruning the sparse sensing matrix. Furthermore, by intrinsically amalgamating the relative frequency based and the proposed factor graph based approach, we conceived a hybrid support identification technique for reducing communication between the sensor nodes and the Fusion Center (FC), while maintaining high-accuracy support identification and simultaneously mitigating the noise contaminating signal reconstruction.**

***Index Terms*—Compressive sensing, support identification, wireless sensor networks, sparse sensing matrix, noise reduction**

I. Introduction

A Sparse signal is one in which most entries adopt a value of zero. In the presence of *a priori* knowledge that a signal is sparse and hence compressible using transform coding, it has been shown in [1] that the signal can be reconstructed from a small number of samples, much lower than dictated by Nyquist's sampling law. In this way, Compressive Sensing (CS) performs data compression jointly with sampling, hence conserving precious communication resources by transmitting and storing a reduced number of measurements [2].

The CS problem can be classified as sparse estimation, support identification, and sparse detection based on the sparse structure of its desired signal, which have ubiquitous applications in wireless communications [3]. In recent years, several detection algorithms have been proposed for doing support identification. The full-search-based Maximum Likelihood (ML) detector is optimal, including an assumption of Gaussian distributed signals, but it suffers from the problem of rapid complexity growth as system size scales [4], hence it is only practical for small systems. The Approximate Message-Passing (AMP) algorithm is an iterative-threshold algorithm based on loopy belief propagation [5]–[7]. It has been shown that the AMP algorithm is capable of doing support identification during the reconstruction of the signals. Another related algorithm designed for signal reconstruction and support identification in CS is the AMP-based Sparse Bayesian Learning (SBL) algorithm. This employs the AMP technique for reducing the complexity of SBL without degrading its performance [8] in the case of dense sensing matrices. However, the performance of both the AMP and AMP-SBL algorithms degrades severely, when the sensing matrix becomes sparse. The Orthogonal Matching Pursuit (OMP) algorithm [9] is more suitable for the sparse sensing matrices considered in this paper. In the OMP algorithm, support identification is employed to solve the least square problem and then reconstructing the signal [10]. Similarly to the Maximum A Posteriori (MAP) support detection algorithm [11] and to the bit-wise MAP support detection algorithm [12], the OMP is a greedy algorithm, which has attracted substantial research attention recently. Like the previously discussed AMP algorithm, these greedy algorithms typically employ dense Gaussian matrices as their sensing matrices in contrast to the sparse binary sensing matrices adopted in this work. However, the authors of [13] have shown that in contrast to the AMP algorithm, the OMP is capable of high-integrity support identification and signal reconstruction in the context of sparse binary sensing matrices. In this paper, we propose a new algorithm for support identification in the case of sparse sensing matrices. The complexity of the proposed approach grows only linearly as the number of sensors and the number of signal entries increases, while offering a support identification performance that approaches that of the ML detector. Therefore it is eminently suitable for realistic system sizes, where the complexity of the ML detector becomes impractical.

In practice, the proposed approach is particularly suitable for spectrum sensing in cognitive radio, active user detection, direction estimation and localization. In addition, there are many other applications that benefit from support identification. Jiang *et al.* [14] introduce a new Autonomous Compressive Spectrum Sensing (ACSS) framework relying on a sophisticated support identification technique. The authors

Corresponding Author: L. Hanzo, J. Chen, S.-X. Ng and R.-G. Maunder are with School of Electronics and Computer Science, University of Southampton, SO17 1BJ, UK. (E-mail: lh@ecs.soton.ac.uk; jc7m17@soton.ac.uk; sxn@ecs.soton.ac.uk; rm@ecs.soton.ac.uk).

T.-Y. Wang is with the Institute of Communications Engineering, National Sun Yat-sen University, Kaohsiung 804, Taiwan (E-mail: tcwang@mail.nsysu.edu.tw).

J.-Y. Wu is with the Institute of Communications Engineering, National Chiao Tung University, Hsinchu 300, Taiwan (E-mail: jywu@cc.nctu.edu.tw).

C.-P. Li is with the Institute of Communications Engineering, National Sun Yat-sen University, Kaohsiung, Taiwan, and also with the Department of Electrical Engineering, National Sun Yat-sen University, Kaohsiung 80424, Taiwan (E-mail: cpli@faculty.nsysu.edu.tw).

TABLE I
CONTRASTING OUR CONTRIBUTION TO THE STATE-OF-THE-ART

	[14]	[19]	[20]	[21]	[22]	[31]	[32]	[34]	[35]	[42]	**This work**
CS	√	√	√	√	√	√	√	√	√	√	√
Support Identification	√	√	√	√	√	√	√	√	√	√	√
Sparse Sensing Matrix							√	√			√
Factor Graph								√			√
Signal Recovery		√				√	√			√	√
MAP algorithm			√		√				√		√
WSNs							√			√	√
Bayesian Inference					√						√

of [15]–[17] employed support identification to wideband spectrum sensing. By contrast, Cohen and Eldar [18] rely on a similar technique for reconstructing the power spectrum of both known and unknown supports. A number of authors [19]–[22] employed support identification for active user detection. Yu *et al.* [23] proposed a Direction Of Arrival (DOA) estimation method based on One-Bit compressed array data by employing support identification. In [24], support identification and sparsity are assumed to be aprior information for improving the signal reconstruction in a multiple-input multiple-output radar system.

Clearly, support identification is an important problem for a whole plethora of applications, even when the estimation of non-zero values is not necessary. Indeed, there are applications where signal reconstruction is not essential, *i.e.* support identification alone is the sole objective [25]. For example, Malioutov *et al.* [26] introduce applications that seek the source location in sensor networks, rather than the source sample values themselves. Multiple-sound-source localization was the design objective in [27], based on providing a Time Difference Of Arrival (TDOA) aided clustering as well as a multipath matching and tracking algorithm. Subset selection in regression associated with sparse vectors [28], [29] is another application, where determining the source location is the only objective.

Furthermore, support identification is also a beneficial step during CS signal reconstruction. For example, in low-cost Wireless Sensor Networks (WSNs), the communication-related energy dissipation can be readily reduced by designing a sensor scheduling protocol by exploiting support identification for reaching the Fusion Center (FC) [30]. Furthermore, [31] illustrates a distributed signal processing algorithm that can reduce the noise and provide reliable signal detection with the aid of support identification. In [32], a relative frequency based support identification technique is proposed for reducing both the data storage and computational requirements of the sensing devices in WSNs, as well as to reduce the communication cost. However, the approach of [32] requires a relatively large number of sensors, which is at odds with one of the basic objectives of CS, namely that of reducing the number of measurements, while minimizing the loss of information [33]. In particular, fewer measurements tend to require fewer sensors, hence leading to a reduced deployment cost, effort and maintenance. To save energy and support efficient calculations, the authors of [34], [35] introduce support identification methods using sparse-graph codes. It is widely recognized that the sensing matrix plays an important role in CS systems, which is used for sampling the sparse signal and it significantly affects the signal recovery performance [36]. Li *et al.* [37]–[39] also prove that using sparse sensing matrices typically reduces the energy consumption. The sparse sensing matrix is also helpful in CS aided WSNs, which is improved in [40], [41]. In a nutshell, WSNs constitute an ideal application scenario for CS and the authors of [42] propose an efficient cluster-sparse reconstruction algorithm based on WSNs with the help of support identification.

Against this background, we conceive a new technique that has an improved support identification accuracy and it is eminently suitable for sparse measurements. We boldly and explicitly contrast our contributions to the state-of-the-art in Table I and detail them below:

1) We propose a new support identification technique based on factor graphs and we separate the support identification from signal reconstruction. The proposed approach supports the use of sparse sensing matrices, which is capable of reducing the energy consumption in CS aided WSNs, as mentioned above.
2) We demonstrate that our proposed scheme retains the advantages of the relative frequency based approach of [32], which avoids the requirement for each sensor to gather and transmit a large vector of measurements, while achieving a higher support identification accuracy. This reduces both the burden of data storage and calculation complexity for the sensing devices.
3) We proposed a novel combination of the relative frequency based and the proposed factor graph based techniques to produce a hybrid scheme, which reduces the communication cost, while maintaining a high support identification accuracy.
4) We show that by employing a sparse sensing matrix that can satisfy the Restricted Isometry Property of the l_1-norm (RIP1) defined and proved in [43], support identification substantially mitigates the signal reconstruction noise.

The rest of this paper is organized as follows. Our proposed system model is introduced in Section II. The proposed factor graph based technique is detailed in Section III, while the communication cost reduction is quantified in Section IV. Our simulation results are presented in Section V, while our conclusions are offered in Section VI.

TABLE II
ASSUMPTIONS IN THIS WORK

Assumption 1	Each entry of the unknown signal support $\boldsymbol{T}$ is uniformly distributed in the range of 1 to N. This assumption is widely adopted in CS systems that perform support identification and signal recovery (e.g., [11], [32]). The proposed system exploits this assumption when the support $\boldsymbol{T}$ is generated.
Assumption 2	Each non-zero signal entry is exploiting real-valued and Independently and Identically Distributed (i.i.d.) according to a Gaussian distribution with zero-mean and a variance of σ_s^2. Similarly, each noise element is real-valued and i.i.d. with zero-mean and a variance of σ_v^2. We know the Gaussian distributed signal entries have been adopted in many previous studies on CS aided WSNs (e.g., [44]–[46]), particularly in applications where WSNs are employed to detect real-life signals such as audio volume, pressure,temperature and so on.
Assumption 3	Each sensor has the knowledge of which signal entries it is observing, while the FC is aware of the sensing matrix $\boldsymbol{\Phi}$. In scenarios like source location, the knowledge of the connections between signal entries and sensors in the sensing matrix could be obtained during the establishment phase of the system model. This assumption is exploited during the decoding phase of the proposed approach.
Assumption 4	We assume that the sparsity level is known *a priori* to the sensors and FC in common with [32]. In a practical CS-based WSN, the sparsity level can be estimated by using residual-based algorithms or cross-validation, which is usually implemented in the FC during the WSNs' training phase [3]. In the proposed scheme, the knowledge of sparsity level K is used during the decoding phase of the FC.
Assumption 5	We assume there is a control overhead or a side-channel which establishes connectivity, maintains synchronization, and it is used for signal acquisition. For the sake of simplicity, the control overhead or side-channel is not simulated in this work. However, we note that [47], [48] provide discussions of these overheads exploited for controlling synchronization and signal acquisition in the FC based WSNs.

II. SYSTEM MODEL

In this section, we introduce the proposed system model as well as the corresponding assumptions, which are listed in Table II.

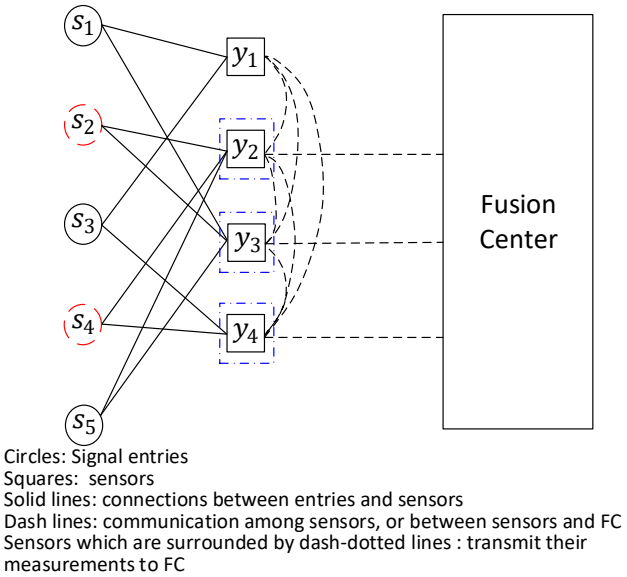

Fig. 1. System model illustrating the relationship between signal entries, sensors and the FC.

In the proposed system, a WSN having M sensors and a FC is employed for support identification and signal estimation for a K-sparse signal $\boldsymbol{s} \in \mathbb{R}^N$ comprising N real-valued entries, of which K ($K \ll N$) are non-zero. Meanwhile, $\boldsymbol{s}$ has an unknown signal support $\boldsymbol{T} \subset \{1,...,N\}$, which contains all indices of the non-zero signal entries.

Based on the CS technique of [49] and in CS-based WSNs, the sparsity of a signal can typically be estimated accurately in practice. Hence, according to Assumption 4, K is known both to the sensors and to the FC in our system. These non-zero entries are assumed to be uncorrelated with each other. Furthermore, each and everyone obeys a Gaussian distribution with zero-mean and the same variance of σ_s^2. Here, our signal entries are modeled using a Gaussian distribution according to the central limit theorem and to enable a fair comparison with the results of [32], which are also assumed to have a Gaussian distribution. Fig. 1 provides an example to illustrate the relationship between the signal entries, sensors and the FC. In this example, the signal entries s_2 and s_4 are marked by red dash lines denoting they are non-zeros. Hence we have $\boldsymbol{T} = \{2,4\}$. The circles in Fig. 1 represent signal entries, each of which is observed by a fixed number of K_s sensors in our system. Squares represent the sensors in the network, where different sensors observe different numbers of signal entries, which are combined together with noise to provide the sensor measurements. More specifically, the measurement model for the set of sensors in the proposed system is given by:

$$\boldsymbol{y} = \boldsymbol{\Phi}\boldsymbol{s} + \boldsymbol{v}, \tag{1}$$

where $\boldsymbol{y} \in \mathbb{R}^M$ is the vector of sensor measurements, with $\boldsymbol{y} = [y_1\ y_2\ y_3\ y_4]^T$ in the example of Fig. 1. Furthermore, $\boldsymbol{\Phi} \in \mathbb{R}^{M \times N}$ ($M < N$) is a sparse sensing matrix, which represents the randomly selected edges in the factor graph selected from the set $\{0,1\}$. For any $,m \in [1,M]$, we define $\boldsymbol{A}_m \subset \{1,...,N\}$ to be the support of the m^{th} row of $\boldsymbol{\Phi}$, which also specifies the indices of all signal entries that are observed by the m^{th}

sensor. For the example in Fig. 1 we have:

$$\mathbf{\Phi} = \begin{bmatrix} 1 & 0 & 1 & 0 & 0 \\ 0 & 1 & 0 & 1 & 1 \\ 1 & 1 & 0 & 0 & 1 \\ 0 & 0 & 1 & 1 & 0 \end{bmatrix}. \tag{2}$$

Finally, $\boldsymbol{s} \in \mathbb{R}^N$ is the signal vector and $\boldsymbol{v} \in \mathbb{R}^M$ is a noise vector, whereby $\boldsymbol{s} = [s_1\ s_2\ s_3\ s_4\ s_5]^T$ and $\boldsymbol{v} = [v_1\ v_2\ v_3\ v_4]^T$.

In the example shown in Fig. 1, we fix the degree of each signal entry to $K_s = 2$, but the degree of the m^{th} sensor ($K_{c,m}, m \in [1, M]$) is random. As a result, each column of $\mathbf{\Phi}$ has a fixed number of non-zero values. The concept of a sparse sensing matrix like this is beneficial for fast compression and signal reconstruction [50] and it also helps perform convenient incremental updates of the signals [51]. Explicitly, a sparse sensing matrix is useful for signal reconstruction because it can satisfy the RIP1 condition defined and proved in [43], [52], which is a sufficient condition for signal reconstruction. In the proposed system, the sensors are capable of sensing, as well as of data processing and communication both with each other and with the FC. After completing the data processing and communication with each other, some of the sensors (as exemplified by the blue dashed dotted squares in Fig. 1) will elect to forward their measurements to the FC, where the final support identification and signal estimation decisions are made. In Fig. 1, dashed lines show the communication among the sensors, as well as between the sensors and the FC.

The detailed actions of our system can be shown using a factor graph, which is composed of Variable Nodes (VNs) and Sensor Nodes (SNs), as exemplified in Fig. 2, for the case where there are $N = 5$ VNs and $M = 4$ SNs. Each VN represents a signal entry and each SN represents a sensor, where the edges connecting these nodes in the graph correspond to the physical connectivity exemplified in Fig. 1. The processing model of Fig. 2 is divided into two parts, where the first part represents the support identification, while the second part is the signal reconstruction.

More specifically, both the sensors and the FC's task of identifying the locations of non-zero entries in the signal entries as well as that of reconstructing the signal is aided by some *a priori* knowledge, such as the length of the signal N, the sparsity K, as well as knowledge of the connections between VNs and SNs.

Fig. 3 shows a flow diagram of our proposed system. The proposed system produces two successive support identifications, followed by the signal estimation, with each estimate informing the next, as shown in Fig. 3. Here, the relative frequency based approach of [32] is used for generating the first estimate of the support $\hat{\boldsymbol{T}}_1$, which has a support size of Z_1 ($K \leq Z_1 \leq N$). This step is completed by the sensors alone, as shown in Fig. 3. In the example of Fig. 2, we assume that the result of relative frequency support identification is $\hat{\boldsymbol{T}}_1 = \{2,4,5\}$, where the corresponding VNs are marked with blue dash-dotted circles. Following this, the sensors that are connected to VNs and are included in $\hat{\boldsymbol{T}}_1$ will forward their measurements to the FC. More explicitly, Sensors 2, 3 and 4 are marked by blue dash-dotted squares in Fig. 2, and will

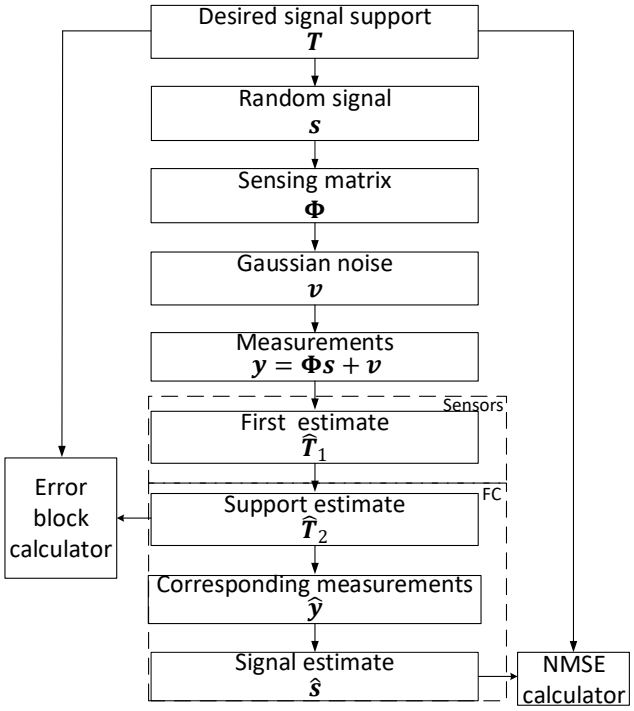

Fig. 3. Flow diagram of the proposed support identification and signal estimation system.

transmit their measurements to the FC, since they are connected to the VNs in $\hat{\boldsymbol{T}}_1$. In the FC, the proposed factor graph based approach is employed for narrowing down the signal estimate and for obtaining the final support identification $\hat{\boldsymbol{T}}_2$ having a smaller size of Z_2 ($K \leq Z_2 \leq Z_1$). In our example of Fig. 2, we have $\hat{\boldsymbol{T}}_2 = \{2,5\}$, which are marked by black dot-dash-dot circles. Following the support identification stage, it can be inferred that some sensor measurements contain only noise and these can be eliminated from consideration during the signal reconstruction stage in order to improve the reconstruction Signal to Noise Ratio (SNR). Hence, only the specific measurements that belong to those sensors that are connected to VNs and are included in the final support identification $\hat{\boldsymbol{T}}_2$ will be used for signal reconstruction, which is performed in the FC, as shown in Fig. 3. Explicitly, observe in Fig. 2 that only y_2 and y_3 are marked by black dot-dash-dot squares, which are used for signal reconstruction. After the signal reconstruction stage, a further narrowing-down is performed by selecting the K reconstructed signal entries having the largest amplitudes, while setting the rest to zeros. A number of special cases arise in the proposed system, depending on the selection of the parameters Z_1 and Z_2, as follows

1) $Z_1 = Z_2 = N$: in this case, all N of the sensors send their measurements to the FC, where signal reconstruction is performed. We refer to this as the conventional approach, where signal reconstruction is performed directly after obtaining the measurements, without performing support identification first.
2) $Z_1 = N$ and $K \leq Z_2 < N$: in this scenario, the

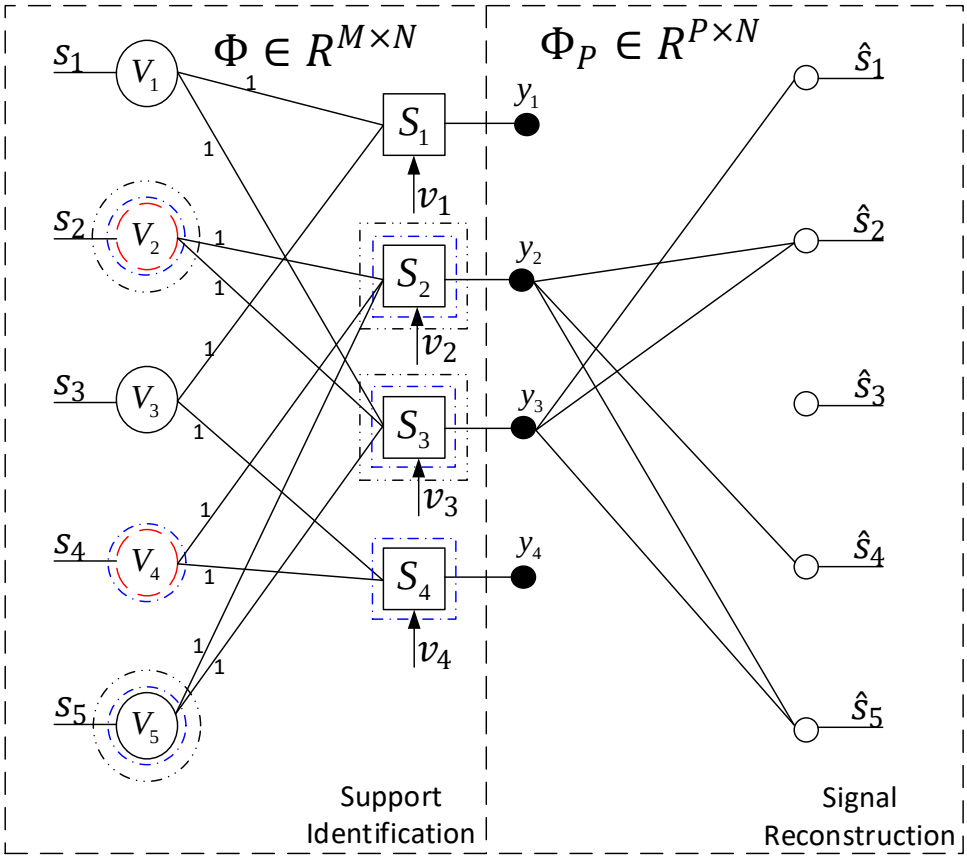

Fig. 2. Factor graph illustrating the processing performed in the proposed system, for the case of $N = 5$ Variable Nodes (VNs) representing the signal entries, of which $K = 2$ have non-zero entries, and each of which is observed by $K_s = 2$ of the $M = 4$ sensors. Here, $Z_1 = 3$ VNs are selected for the first estimate of the support marked by dash-dotted lines, before $Z_2 = 2$ VNs are selected for the final support identification marked by dot-dash-dot lines.

relative frequency based approach is skipped and only our proposed factor graph based technique is used for support identification.

3) $K \leq Z_1 < N$ and $K \leq Z_2 < Z_1$: this is the general case, where the relative frequency based approach is applied first, followed by the proposed factor graph based approach invoked for support identification.
4) $Z_1 = Z_2 < N$: in this case, the use of $Z_1 = Z_2$ implies that after we achieve the first estimate using the relative frequency based approach, we immediately perform signal reconstruction. In this case, the proposed factor graph based approach is skipped and only the relative frequency based approach is used for support identification, as characterized in [32].

During the support identification action, there are two different types of errors, namely false positives and false negatives[1]. False positive is caused by identifying a non-zero entry as a zero entry, while false negative is the opposite of false positive, which occurs when a zero entry is identified as a non-zero entry. There are three sources of loss associated with signal reconstruction, namely false positives during support identification, false negatives during support identification and the noise within the measurements. Of these, it is false positives that lead to the most grave loss, because they result in the desired signal entries being erased. By contrast, false negatives and noise have less grave effects since they both represent noise in the reconstructed signal, rather than the residuals. Furthermore, because false negatives are less harmful than false positives [32], this motivates setting Z_2 to be slightly larger than K, which has the effect of increasing the false negative rate, but reducing the false positive rate and hence improving the overall signal reconstruction quality. However, setting Z_2 to be too large will lead to an excessive number of false negatives and so a beneficial trade-off must be found.

[1]False positives and false negatives correspond to misidentification and false alarms respectively, as used in [32].

III. Proposed Factor Graph Based Approach

Here we conceive a new support identification technique with the aid of factor graphs, the belief propagation algorithm, MAP algorithm and an iterative exchange of soft *extrinsic* information. We utilize a pair of decoders in the FC, namely the Variable Node Decoder (VND) and the Sensor Node Decoder (SND), which are further decomposed into two parts. The iterative decoding operation exchanging *extrinsic* information between the two decoders is shown in Fig. 4, where

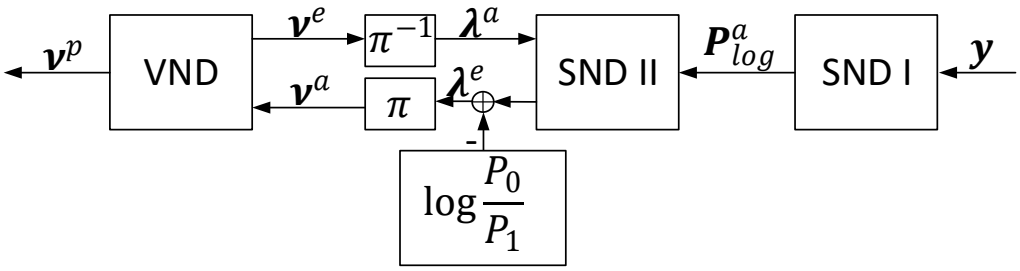

Fig. 4. The iterative decoding process performed between the VND and SND.

$\boldsymbol{P}^a_{log}$ of length $\sum_{m=1}^{M}(\sum_{k=0}^{\min\{K,K_{c,m}\}}\binom{K_{c,m}}{k})$ represents the logarithmic conditional probabilities associated with the SND, which contains all SNs' logarithmic conditional probabilities. Furthermore, $\boldsymbol{\lambda}^a$ and $\boldsymbol{\lambda}^e$ denote the vectors of $N \cdot K_s$, which store all SNs' *a priori* and *extrinsic* Logarithmic Likelihood Ratios (LLRs), respectively, while $\boldsymbol{\nu}^a$, $\boldsymbol{\nu}^e$ and $\boldsymbol{\nu}^p$ are the vectors of length $N \cdot K_s$ *a priori* LLRs, $N \cdot K_s$ *extrinsic* LLRs and N *a posteriori* LLRs of the VND, respectively.

For the proposed approach to work successfully, the FC has the knowledge of the signal length N, the sensing matrix $\boldsymbol{\Phi}$ and the sparsity variable K. Furthermore, according to Assumption 3, each SN has the knowledge of K and knows which VNs it observes. The first step of support identification is based on the measurements $\boldsymbol{y}$, which are used for computing the logarithmic conditional probabilities $\boldsymbol{P}^a_{log}$ that are computed by the 'SND I' block shown in Fig. 4. The second step relies on the 'SND II' computing the vector of $N \cdot K_s$ *extrinsic* LLRs $\boldsymbol{\lambda}^e$ based on the *a priori* LLRs $\boldsymbol{\lambda}^a$ and $\boldsymbol{P}^a_{log}$, as seen in Fig. 4. During the iterative information exchange between SND II and VND, $\boldsymbol{\lambda}^a$ will be initialized to an all-zero vector of length $N \cdot K_s$ before the first iteration. More explicitly, the $N \cdot K_s$ *extrinsic* LLRs $\boldsymbol{\lambda}^e$ are computed by subtracting the scalar constant $\log\frac{P(0)}{P(1)}$ from each element in the vector output of SND II, as shown in Fig. 4. The $N \cdot K_s$ *extrinsic* LLRs of SND become the *a priori* LLRs $\boldsymbol{\nu}^a$ for the VNs after going through an interleaver (π), which represents the connectivity in the factor graph and is explained in the [53]. The VND then computes the $N \cdot K_s$ *extrinsic* LLRs $\boldsymbol{\nu}^e$ based on the $N \cdot K_s$ *a priori* LLRs $\boldsymbol{\nu}^a$ and then forwards them to SND II. The iterative decoding operations exchanging soft extrinsic information between SND II and the VND are repeated until the maximum affordable number of iterations is exhausted. More explicitly, the iterations between the SNs and VNs will be repeated until the *extrinsic* LLRs $\boldsymbol{\nu}^e$ convergence, or until an iteration limit is reached, whereupon the decoding is terminated. The final step is to sort the *a posteriori* LLRs ($\boldsymbol{\nu}^p$) of the VNs in order to identify the specific VNs that are most likely to have non-zero values. Then, the indices of the Z_2 most negative LLRs are selected to provide the support identification $\hat{\boldsymbol{T}}_2$. The detailed description of the SND and VND operations will be provided in the following subsections.

A. SND I Update

The SND I block of Fig. 4 performs calculations pertaining to each of the M sensors. The detailed process discussed in this section is based on the operation of a single SN, with all other SNs in the SND performing the same process in parallel to it.

As mentioned before, the FC has the knowledge of both the SNs' connections and of the sparsity K. Based on this knowledge, all permutations of the SN-VN connections can be computed for all SNs. The SND I block aims for calculating the logarithmic conditional probability for each permutation. Let us consider the example based on SN 2 of Fig. 2, which may be represented by the permutation matrix

$$\mathbf{Q} = \begin{bmatrix} 0 & 0 & 0 & 0 & 1 & 1 & 1 \\ 0 & 0 & 1 & 1 & 0 & 0 & 1 \\ 0 & 1 & 0 & 1 & 0 & 1 & 0 \end{bmatrix}. \tag{3}$$

The permutation matrix $\mathbf{Q}$ has $K_{c,2}$ rows and up to $2^{K_{c,m}}$ columns, where the exact number of columns is $\sum_{k=0}^{\min\{K,K_{c,2}\}}\binom{K_{c,2}}{k}$. Each column of the matrix represents a permutation and each row represents a different one of the possibilities for a specific connected signal entry of the SN. In this example, the signal is composed of $N = 5$ signal entries, with $K = 2$ non-zero entries, and SN 2 observes $K_{c,2} = 3$ of the signal entries. Although SN 2 is connected to $K_{c,2} = 3$ entries, only a maximum of $K = 2$ of them can adopt non-zero values. Alternatively, we may encounter the scenario that only one or none of the connected signals is non-zero. The hypotheses of how many connected entries are non-zero for this example are therefore given by the vector $\bar{\boldsymbol{h}} = [0 \quad 1 \quad 2]$. The hypotheses are also reflected in the permutation matrix $\mathbf{Q}$. The elements of the first column $\mathbf{Q}$ are all zero because it considers the hypothesis that all VNs connected to SN 2 have zero values. Furthermore, the second column of the matrix represents a possible permutation in which the 5^{th} VN of Fig. 2 observed by SN 2, has a non-zero value, while the other VNs connected to SN 2 have zero values. Comparing the hypotheses vector $\bar{\boldsymbol{h}}$ to the permutation matrix, $\mathbf{Q}$ reveals that several permutations can share a specific hypothesis for a given number of connected non-zero values. The following steps detail the mathematical calculation of the logarithmic conditional probabilities.

Based on the knowledge of connections, on the length N

of the signal and the sparsity K, the hypothesis matrix $\bar{\boldsymbol{h}}$ can be found for each SN. The probability of a given hypothesis $h, h \in [0, \min\{K, K_{c,m}\}]$ can be calculated with the help of the hypergeometric distribution as:

$$P(h) = \frac{\binom{K}{h}\binom{N-K}{K_{c,m}-h}}{\binom{N}{K_{c,m}}}, \tag{4}$$

where h is one of the possible hypotheses in $\bar{\boldsymbol{h}}$, $\bar{\boldsymbol{h}} = [0, ..., \min\{K, K_{c,m}\}]$. Hence, $\boldsymbol{P}(\bar{\boldsymbol{h}}) = [P(h=0), P(h=1), \cdots, P(h=\min\{K, K_{c,m}\})]$.

Since the non-zero signal entries are Gaussian distributed with zero mean, and variance σ_s^2 and because the noise also obeys the Gaussian distribution with zero mean and variance σ_v^2, the Gaussian probability density function can be invoked for calculating the conditional probability of the measurement for hypotheses h

$$P(y_m|h) = \frac{e^{-\frac{y_m^2}{2\sigma_y^2}}}{\sqrt{2\pi\sigma_y^2}}, \tag{5}$$

where we have $\sigma_y^2 = h \cdot \sigma_s^2 + \sigma_v^2$, and y_m is the measurement of the m^{th} ($m \in [1, M]$) SN. Here, we have the vector $\boldsymbol{P}(y_m|\bar{\boldsymbol{h}}) = [P(y_m|h=0), \cdots, P(y_m|h=\min\{K, K_{c,m}\})]$. Next we may use Bayes' law to convert $P(y_m|h)$ ($h \in [0, \cdots, \min\{K, K_{c,m}\}]$) to the joint probability

$$P(y_m, h) = P(y_m|h)P(h), \tag{6}$$

and for computing the conditional probability

$$P(h|y_m) = \frac{P(y_m|h) \cdot P(h)}{\sum_{h=0}^{\min\{K, K_{c,m}\}} P(y_m|h) \cdot P(h)}. \tag{7}$$

The probabilities of the hypotheses among all permutations that have the corresponding weight can be computed as

$$P^a(h|y_m) = \frac{P(h|y_m)}{n_{uj}}, \tag{8}$$

where $P(h|y_m)$ is the conditional probability for the hypothesis h in the vector $\bar{\boldsymbol{h}}$ and $j = h$ here. Again, a specific hypothesis may correspond to more than one of the permutations in the matrix $\mathbf{Q}$. To calculate the conditional probability of each permutation, the probability of the corresponding hypothesis should be divided by $n_{uj}, j \in [0, \min\{K, K_{c,m}\}]$, where n_{uj} is an element of the vector $\boldsymbol{n_u} = [n_{u0} ... n_{uj} ... n_{u\min\{K, K_{c,m}\}}]$, which quantifies the number of permutations sharing the same hypothesis h. In the example above, SN 2 of Fig. 2 has three legitimate hypotheses $\bar{\boldsymbol{h}} = [0, 1, 2]$, with each corresponding to different numbers of permutations, according to $\boldsymbol{n_u} = [1, 3, 3]$.

Then we can convert $P^a(h|y_m)$ to a logarithmic probability according to

$$P_{log}^a(h|y_m) = \log[P(h|y_m)]. \tag{9}$$

As mentioned above, the permutations corresponding to the same hypothesis share the same probability. In order to obtain a vector that contains all logarithmic conditional probabilities for all permutations, we should allocate the logarithmic probabilities for each permutation. Let us assume that we have $\boldsymbol{P}_{log}^a(\bar{\boldsymbol{h}}|y_m) = [P_{log}^a(h=0|y_m) \quad P_{log}^a(h=1|y_m) \quad P_{log}^a(h=2|y_m)]$ for the above example. The permutations corresponding to the hypothesis of value 1 share $P_{log}^a(h=1|y_m)$, while those corresponding to the hypothesis of value 2 share $P_{log}^a(h=2|y_m)$. Hence, the final result for our example above is $\boldsymbol{P}_{log}^a(\mathbf{Q}|y_m) = [P_{log}^a(h=0|y_m) \quad P_{log}^a(h=1|y_m) \quad P_{log}^a(h=1|y_m) \quad P_{log}^a(h=1|y_m) \quad P_{log}^a(h=2|y_m) \quad P_{log}^a(h=2|y_m) \quad P_{log}^a(h=2|y_m)]$. Here, we use $P_{log}^a(\boldsymbol{Q}_g|y_m)$ to represent a log-probability for one permutation, and $\boldsymbol{Q}_g$ is the g^{th} column of $\mathbf{Q}$, where we have $g \in [1, \sum_{k=0}^{\min\{K, K_{c,m}\}} \binom{K_{c,m}}{k}]$. Furthermore, $\boldsymbol{P}_{log}^a(\mathbf{Q}|y_m)$ is a vector that contains all conditional probabilities of the m^{th} SN, and $\boldsymbol{P}_{log}^a(\mathbf{Q}|y_m)$ is part of $\boldsymbol{P}_{log}^a$, which is composed of vectors for each of the M sensor nodes.

B. SND II Update

Once the SND I block of Fig. 4 has computed the logarithmic conditional probabilities $\boldsymbol{P}_{log}^a$, the $N \cdot K_s$ *extrinsic* LLRs $\boldsymbol{\lambda}^e$ will be computed by SND II. In this section, we elaborate on this process by describing the operation of a single SN, with all other SNs also performing the same process in parallel.

More explicitly, the set of *extrinsic* LLRs $\boldsymbol{\lambda}_m^e$ of m^{th} SN of length $K_{c,m}$ can be computed based on the vector of $\sum_{k=0}^{\min\{K, K_{c,m}\}} \binom{K_{c,m}}{k}$ conditional probabilities $\boldsymbol{P}_{log}^a(\mathbf{Q}|y_m)$ of m^{th} SN and the set of $K_{c,m}$ *a priori* LLRs $\boldsymbol{\lambda}_m^a$, where $m \in [1, M]$ and $\boldsymbol{\lambda}_m^a$ are initialized to a zero vector before the first iteration.

The computation commences by using the conditional probability $P_{log}^a(\boldsymbol{Q}_g|y_m)$ and *a priori* LLRs $\boldsymbol{\lambda}_m^a$ to calculate the *a posteriori* probability $P_{log}^p(\boldsymbol{Q}_g|y_m)$. More specifically, each SN considers all possible permutations of its connections, with each permutation having its own corresponding *a priori* probability in the vector $\boldsymbol{P}_{log}^a(\mathbf{Q}|y_m)$. Each permutation computes its corresponding *a posteriori* probability according to

$$P_{log}^p(\boldsymbol{Q}_g|y_m) = P_{log}^a(\boldsymbol{Q}_g|y_m) - \sum_{n \in N'(m)} \lambda_{n \to m}^a, \tag{10}$$

where $P_{log}^p(\boldsymbol{Q}_g|y_m)$ is the *a posteriori* probability of the g^{th} permutation in the g^{th} column of the $\mathbf{Q}$ corresponding to the particular *a priori* probability $P_{log}^a(\boldsymbol{Q}_g|y_m)$. Furthermore, $\lambda_{n \to m}^a$ is the *a priori* LLR provided by $\boldsymbol{\lambda}_m^a$ that represents the *a priori* LLR gleaned from the n^{th} VN and forwarded to the m^{th} SN. Furthermore, $N'(m)$ represents a set that contains all VNs connected to the m^{th} SN and that have non-zero values in the $\boldsymbol{Q}_g$, where $\boldsymbol{Q}_g$ is the g^{th} column of $\mathbf{Q}$, which represents a specific permutation of the m^{th} SN. The *a posteriori* probabilities of all permutations comprise the *a posteriori* probabilities vector $\boldsymbol{P}_{log}^p(\mathbf{Q}|y_m)$ of the m^{th} SN. Following this, the *a posteriori* probabilities can be converted into *a posteriori* LLRs according to

$$\begin{aligned} \lambda_{n \to m}^p = &\max^*[\boldsymbol{P}_{log}^p(\boldsymbol{Q}_{n|_{Q_{n,g}=0}}|y_m)] \\ &- \max^*[\boldsymbol{P}_{log}^p(\boldsymbol{Q}_{n|_{Q_{n,g}=1}}|y_m)] \end{aligned}. \tag{11}$$

where $\lambda_{n \to m}^p$ is the corresponding *a posteriori* LLR of $\lambda_{n \to m}^a$, with $n \in N(m)$ and $N(m)$ denoting the set of VNs which are

connected to the m^{th} SN of length $K_{c,m}$. Additionally, $\boldsymbol{Q}_n$ is the n^{th} row of the permutation matrix $\mathbf{Q}$, which represents all possibilities for the n^{th} VN, while $Q_{n,g}$ is the n^{th} row and g^{th} column of $\mathbf{Q}$. Here, $\boldsymbol{P}^p_{log}(\boldsymbol{Q}_{n|_{Q_{n,g}=0}}|y_m)$ denotes a vector provided for the n^{th} VN by $\boldsymbol{P}^p_{log}$, which contains *a posteriori* probabilities, whose corresponding permutations have zero values in the n^{th} row of the permutation matrix $\mathbf{Q}$. Furthermore, $\boldsymbol{P}^p_{log}(\boldsymbol{Q}_{n|_{Q_{n,g}=0}}|y_m)$ is a vector of inputs to the Jacobian logarithm, where this function can be extended to accept this number of inputs by exploiting its associative property. Likewise, $\boldsymbol{P}^p_{log}(\boldsymbol{Q}_n|_{Q_{n,g}=1}|y_m)$ represents a vector provided for the n^{th} VN by $\boldsymbol{P}^p_{log}$, which contains *a posteriori* probabilities whose corresponding permutations have non-zero values at the n^{th} row of permutation matrix $\mathbf{Q}$.

Here, $\max^*$ represents the Jacobian logarithm defined in [54], which is given for two arguments by

$$\begin{aligned}\max^*(a,b) &= \log(e^a + e^b) \\ &= \max(a,b) + \log(1 + e^{-|a-b|}).\end{aligned} \tag{12}$$

This formula may be readily extended to more arguments by exploiting its associative property. For instance, when the arguments are extended to three, the $\max^*$ function is defined as $\max^*(a,b,c) = \max^*(\max^*(a,b),c)$.

Finally, the set of $K_{c,m}$ *extrinsic* LLRs $\boldsymbol{\lambda}^e_m$ are computed by subtracting the *a priori* LLRs ($\boldsymbol{\lambda}^a_m$) from the *a posteriori* LLRs ($\boldsymbol{\lambda}^p_m$) according to

$$\boldsymbol{\lambda}^e_m = \boldsymbol{\lambda}^p_m - \boldsymbol{\lambda}^a_m - \log\frac{P_0}{P_1}, \tag{13}$$

where P_0 is the probability of having zero-valued entries in the signal $\boldsymbol{s}$, and P_1 is the probability of non-zero entries. Here, based on Assumptions 3 and 4, the decoder has the knowledge of signal length N (number of columns of the sensing matrix $\boldsymbol{\Phi}$) and sparsity K, which means that $P_0 = \frac{K}{N}$ and $P_1 = 1 - P_0$ are known. It is necessary to subtract $\log\frac{P_0}{P_1}$ here, in order to avoid positive feedback, which is caused by the VND preserving the knowledge provided by the SND and returning it back to the SND.

C. VND Update

The VND block of Fig. 4 converts the vector of $N \cdot K_s$ *a priori* LLRs $\boldsymbol{\nu}^a$ into the vector of N *a posteriori* LLRs $\boldsymbol{\nu}^p$ and $N \cdot K_s$ *extrinsic* LLRs $\boldsymbol{\nu}^e$. Here, for the n^{th} ($n \in [1,N]$) VN, the *a posteriori* LLR ν^p_n and set of K_s *extrinsic* LLRs $\boldsymbol{\nu}^e_n$ can be computed from

$$\nu^p_n = \sum_{m \in \boldsymbol{M}(n)} \nu^a_{m\to n}, \tag{14}$$

$$\nu^e_{m\to n} = \sum_{m' \in \boldsymbol{M}(n)\setminus\{m\}} \nu^a_{m'\to n}, \tag{15}$$

where $\nu^a_{m\to n}$ and $\nu^a_{m'\to n}$ are the *a priori* LLRs from the m^{th} and m'^{th} SNs to the n^{th} VN respectively that are provided by $\boldsymbol{\nu}^a_n$, which is the set of K_s *a priori* LLRs for the n^{th} VN. Here, $\boldsymbol{M}(n)$ denotes the set of SNs that are connected to the n^{th} VN and $\boldsymbol{M}(n)\setminus\{m\}$ represents the subset of $\boldsymbol{M}(n)$ that excludes the m^{th} SND.

IV. Communication Cost

In a WSN, the communication between sensors and the FC predetermines the energy consumption, reliability and interference imposed by the system. In our proposed scheme shown in Fig. 1, the communication between sensors mainly takes place in the process of finding the first estimate ($\hat{\boldsymbol{T}}_1$) of the support. After determining the first estimate of $\hat{\boldsymbol{T}}_1$, the sensors that are connected to VNs belonging to $\hat{\boldsymbol{T}}_1$ will forward their measurements to the FC. Following this, the factor graph operations and signal reconstruction can be performed in the FC. Again, the flow of the process is shown in Fig. 3.

In the relative frequency based approach of [32], the communication between sensors occurs when active sensors broadcast their binary local decisions to the other sensors. The local decision of the m^{th} SN is made based on its measurement y_m [32] according to

$$u_m(y_m) = \begin{cases} 1 & \text{if } |y_m| > \eta \triangleq L_0^{-1}(\frac{\pi_0}{\pi_1}) \\ 0 & \text{otherwise} \end{cases}, \tag{16}$$

where we have $\pi_0 = \frac{C^{N-K_{c,m}}_K}{C^N_K}$,$\pi_1 = \frac{\sum_{j=1}^{\min(K,K_{c,m})} C^{K_{c,m}}_j C^{N-K_{c,m}}_{K-j}}{C^N_K}$ and $L_0 = L|_{\mathbb{R}+\cup\{0\}} \triangleq \sum_{j=1}^{\min(K,K_{c,m})} \frac{C^{K_{c,m}}_j C^{N-K_{c,m}}_{K-j}}{\sum_{j'=1}^{\min(K,K_{c,m})} C^{K_{c,m}}_{j'} C^{N-K_{c,m}}_{K-j'}}$ $\times \sqrt{\frac{\sigma_v^2}{j\sigma_s^2+\sigma_v^2}} \exp(-\frac{j\sigma_s^2 y_m^2}{2\pi\sigma_v^2(j\sigma_s^2+\sigma_v^2)})$, as detailed in [32].

When the local decision of $u_m(y_m) = 1$ is made, the sensor is activated, and it will broadcast its local binary decision to the other sensors, otherwise it should remain silent. The expected communication cost of the m^{th} SN may be quantified as [32]

$$\beta_i \triangleq \alpha_1 P(m \in \boldsymbol{I}) + \alpha_2 P(m \in \boldsymbol{E}), \tag{17}$$

where α_1 is the communication cost related to the relative frequency based approach of finding the first estimate of $\hat{\boldsymbol{T}}_1$, which is followed by broadcasting the local binary decisions to all other sensors, if the m^{th} sensor is active. By contrast, α_2 is the communication cost between the sensors and the FC after arriving at the first estimate $\hat{\boldsymbol{T}}_1$, where the sensors connected to the Z_1 number of VNs forward their measurements to the FC, as shown in Fig. 3. Here, $\boldsymbol{I}$ is the set of sensors that are active, while $\boldsymbol{E}$ is the set of sensors that forward their measurements to the FC. $P(m \in \boldsymbol{I})$ is the probability that the m^{th} SN is active, while $P(m \in \boldsymbol{E})$ is the probability that the m^{th} SN will forward its measurement to the FC. In reality, α_1 is always lower than α_2 [32], since α_1 is the communication cost associated with transmitting one-bit messages, while α_2 is the communication cost associated with transmitting measurements that are encoded by a multi-bit messages. The communication cost associated with a variety of scenarios will be characterized in Section V. Here, the computation performed in the sensors consumes extra power and increases the chip area. However, this may be expected to be limited, since the computations of local decisions in the sensors are made according to the simple equations 16. More specifically, the calculation of the 'relative frequency' involves additions and one division, which can be expected to consume only a small amount of extra power. However, the extra communication also consumes power, bandwidth

and time-frequency resources. As discussed in [56], it may be expected that the power consumption of communication is several times higher than that of the sensor computation.

V. Simulation Results

In this section, simulation results are provided to demonstrate the efficiency of the proposed factor graph based approach and to compare its performance to various benchmarks. Throughout our investigations, we employ different approaches to do support identification, and utilize weight l_1 minimization to do signal recovery for all approaches. We set the weighted l_1-norm minimization values $w_n = 0.5$ if $n \in \hat{\boldsymbol{T}}_2$, otherwise, $w_n = 1$ if $n \notin \hat{\boldsymbol{T}}_2$. The method of weight l_1 minimization is introduced in [55]. Weighted l_1 minimization uses small weights to reduce the penalties of 'expected' large entries of the signal in the weighted objective function [57], based on the results of support identification.

As mentioned in Section II, false negatives may be deemed less harmful than false positives. Furthermore, in cases where $Z_2 > K$, false negatives can happen independently of false positives. Hence, we focus our attention on characterizing the errors caused by false positives in our simulations by comparing $\hat{\boldsymbol{T}}_2$ to $\boldsymbol{T}$ shown in the flowchart of Fig. 3. More specifically, we use the notation F_b to represent that particular fraction of blocks, in which not all non-zero entries of the signal are identified. Hence F_b may be termed as the support identification failure probability. Furthermore, the quality of signal reconstruction can be quantified by the Normalized Mean Square Error (NMSE) defined as [32]:

$$\text{NMSE} \triangleq E\left\{\frac{\|s-\hat{s}\|^2}{\|s\|^2}\right\}. \tag{18}$$

As shown in Fig. 5, the complexity of the proposed factor graph based approach grows at a modest rate upon increasing the WSN size. By contrast, the complexity of the ML algorithm escalates at a significantly higher rate upon increasing the WSN size and it becomes orders of magnitude higher than that of the proposed scheme. We may observe that while the complexity of the proposed scheme reduces upon increasing δ, the complexity of the ML scheme increases with δ.

Fig. 6 presents a comparison between the proposed factor graph based approach and the conventional OMP algorithm. More specifically, the false positive rate performance F_b of the proposed factor graph based approach can be seen to be significantly better than the OMP algorithm for $\delta = \frac{1}{5}$, along with $K = 5$, $K_s = 2$, $Z_2 = 8$ and SNR = 24 dB. We note that when increasing the value of δ, the advantage of the proposed factor graph based approach reduces at small N values. Furthermore, the performance of the OMP algorithm becomes similar to the proposed factor graph based approach at large δ and N values. Hence, we may conclude that the factor graph based approach has the greatest benefit in situations where δ is small, and it is marginally better than the OMP algorithm at large δ and moderate N values.

In the following investigations, we set $N = 500$, $K = 5$, $\delta = \frac{2}{5}$ and $Z_2 = 8$. In this case, the AMP algorithm achieves false positive rates F_b of 100%, irrespective of the SNR

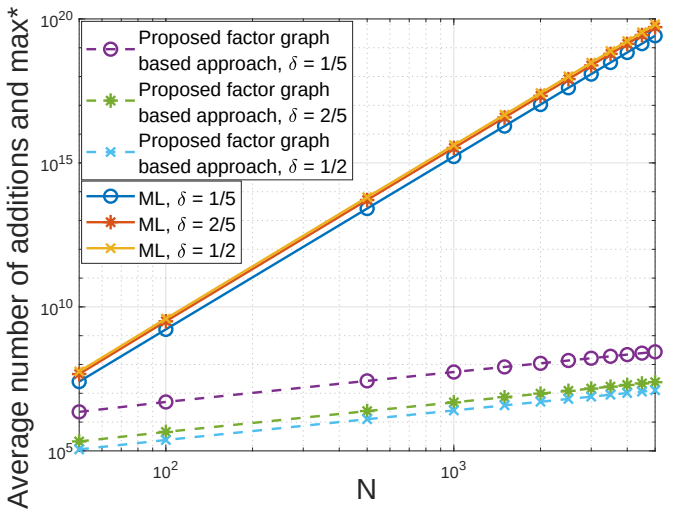

Fig. 5. Complexity of calculating the average number of additions and max* with $K = 5$ and $K_s = 2$.

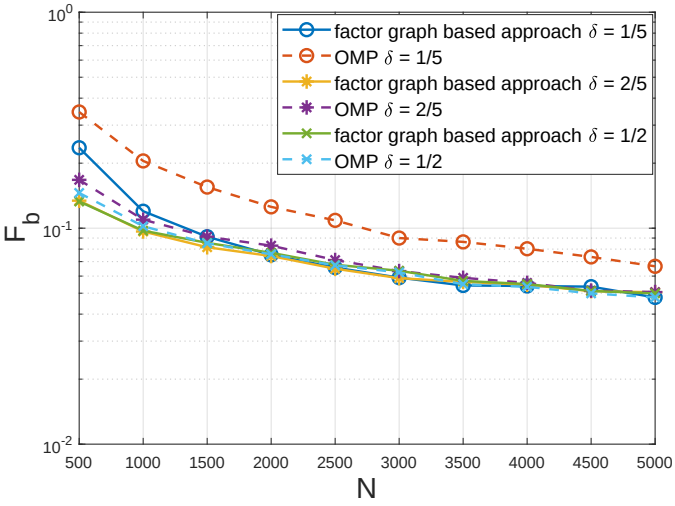

Fig. 6. F_b of factor graph based approach and OMP algorithm with $K = 5$, $K_s = 2$, $Z_2 = 8$ and SNR = 24 dB.

because it cannot support the sparse sensing matrices that are employed in our system. Fig. 7 characterizes the false positive rate F_b of the proposed approach and of the relative frequency based approach for different values of K_s. Fig. 7 shows that the false positive rate F_b of neither the factor graph based approach nor of the relative frequency based approach is influenced significantly by the value of K_s. Fig. 8 characterizes the performance of the hybrid approach, which amalgamates both the relative frequency based approach and the proposed factor graph based technique. As expected, the false positive rate F_b results of the hybrid approach do not change significantly when increasing the value of K_s. A small K_s value indicates that a signal entry is only observed by a small number of sensors, which in turn results in a lower computational complexity than high K_s values. Hence, it is preferred if reliable support identification can be achieved for the case of small K_s. Fig. 8 also shows the impact of different

Z_1 values for the hybrid approach. When increasing the value of Z_1, the false positive rate F_b of the hybrid approach can be seen to exhibit little improvement. Here, it is preferred if reliable support identification can be achieved using a small Z_1 value because of the associated reduction in communication cost. Motivated by achieving a low computational complexity in support identification, Fig. 9 provides a comparison of the different approaches for the case of $K_s = 2$. In situations where only the locations of non-zero entries are needed, the objective is that of attaining a high support identification accuracy. As shown in Fig. 9, the support identification success probability of the proposed factor graph based approach is better than that of the benchmark methods, as manifested in terms of a lower false positive rate F_b. The hybrid approach requires about 3 dB higher SNR than the proposed factor graph aided approach, when aiming for a false positive rate of $F_b = 0.1$. In turn, the hybrid technique offers a further 3 dB gain compared to the relative frequency based approach at a false positive rate of $F_b = 0.1$, as shown in Fig. 9. Meanwhile, the OMP algorithm needs about 6 dB higher SNR to achieve $F_b = 0.1$ compared to the proposed factor graph based approach.

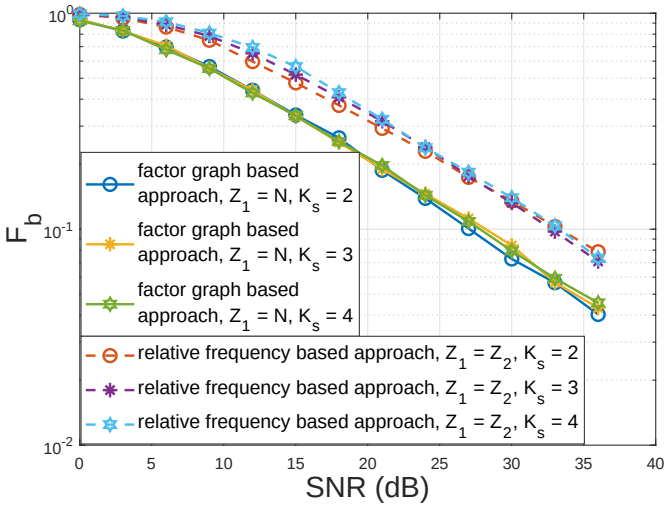

Fig. 7. F_b of factor graph based approach and relative frequency based approach with $N = 500$, $K = 5$, $\delta = \frac{2}{5}$ and $Z_2 = 8$.

The performance of signal reconstruction can be characterized by the NMSE. As shown in Fig. 10 and 11, the signal reconstruction NMSE performance will be significantly improved as the value of K_s is increased both for the proposed factor graph based approach, for the relative frequency based approach and the hybrid approach. This is in contrast to the false positive rate F_b, which has only marginal dependence on the value of K_s. Increasing K_s from 2 to 3 significantly improves the NMSE performance but results in an error floor, as shown in Fig. 10 and 11. Increasing K_s further to 4 eliminates this error floor and further improves the NMSE performance. We may attribute the significant effect of K_s upon NMSE to the observation that higher values of K_s provide more opportunities to detect the specific sensors, which are observing non-zero entries. This is beneficial when performing signal reconstruction even in the case where support identification did not find all the locations of non-zero entries. As shown in Fig. 10, the signal reconstruction NMSE of the proposed factor graph based approach is reduced to -35 dB, when the false positive rate F_b is 0.1. Hence, we may conclude that the proposed scheme can tolerate a false positive rate of as high as 0.1. It also may be observed in Fig. 11 that the signal reconstruction performance of the hybrid approach does not change substantially with the value of Z_1. In situations where the reconstructed signal needed, the objective becomes that of attaining a high signal reconstruction accuracy. Additionally, Fig. 12 compares the signal reconstruction NMSE performance of the various approaches considered for the cases where each signal entry is observed by $K_s = 4$ sensors. Fig. 12 includes results for the conventional approach, which performs signal reconstruction directly after receiving the measurements, i.e. without employing support identification first. It may be observed that the proposed factor graph based approach achieves the best performance, offering

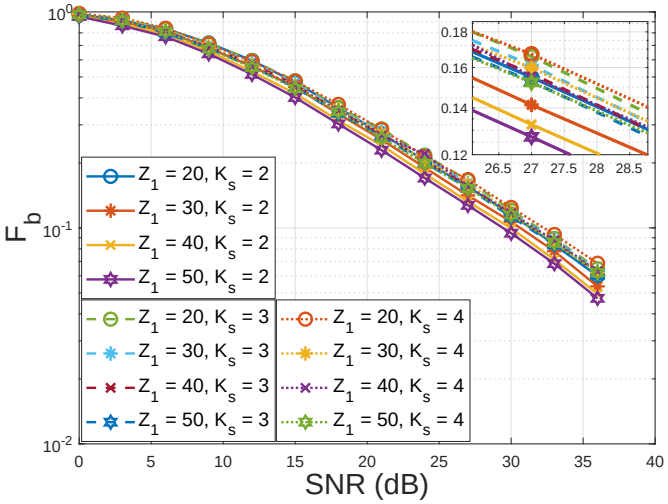

Fig. 8. F_b of hybrid approach with $N = 500$, $K = 5$, $\delta = \frac{2}{5}$ and $Z_2 = 8$.

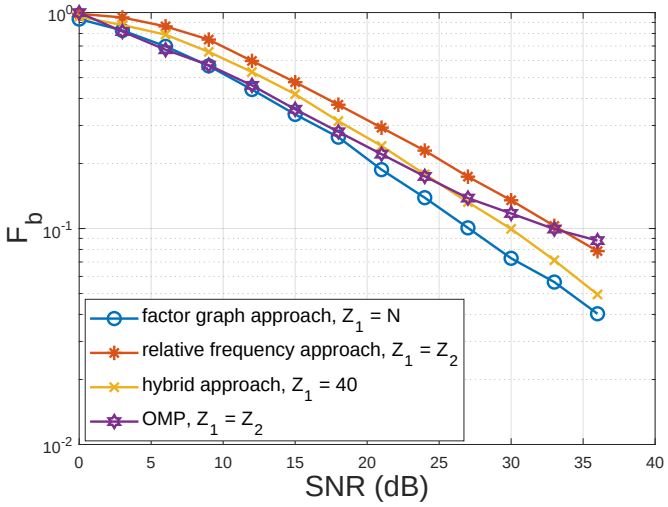

Fig. 9. F_b of different approaches with $N = 500$, $K = 5$, $\delta = \frac{2}{5}$, $Z_2 = 8$ and $K_s = 2$.

about 4 dB SNR gain compared to the conventional approach, at a signal reconstruction NMSE of about -40 dB. Both the hybrid approach and the relative frequency based approach can achieve a similar signal reconstruction NMSE performance to that of the proposed factor graph based approach, while the OMP algorithm has a slightly better performance than the conventional approach. According to these results, we may conclude that support identification assists in mitigating the detrimental effect of noise and significantly improves signal reconstruction.

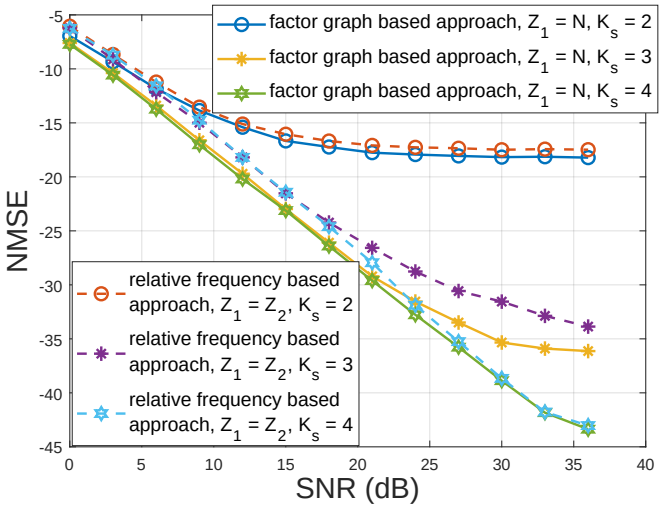

Fig. 10. NMSE of factor graph based approach and relative frequency based approach with $N = 500$, $K = 5$, $\delta = \frac{2}{5}$ and $Z_2 = 8$.

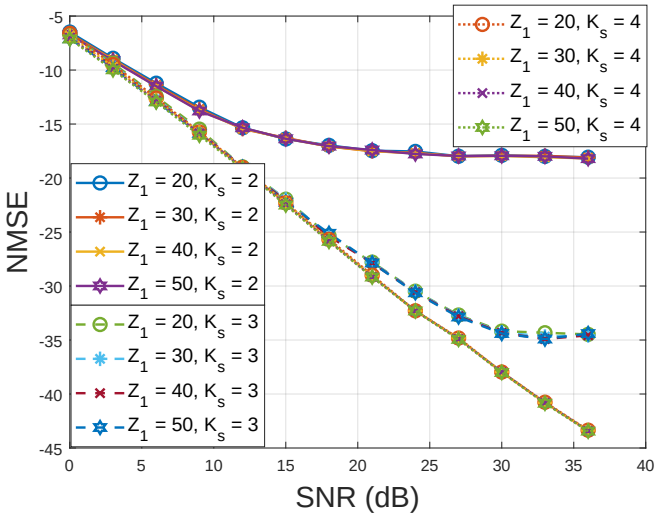

Fig. 11. NMSE of hybrid approach with $N = 500$, $K = 5$, $\delta = \frac{2}{5}$ and $Z_2 = 8$.

Fig. 13 shows the average communication cost of the different approaches, for the case where the communication cost between sensors is quantified by the parameter of $\alpha_1 = 1$ and the communication cost between sensors and FC is quantified by the parameter of $\alpha_2 = 32$. Here, it may be observed that the relative frequency based approach and the proposed hybrid approach significantly reduce the associated communication cost relative to the conventional and the proposed

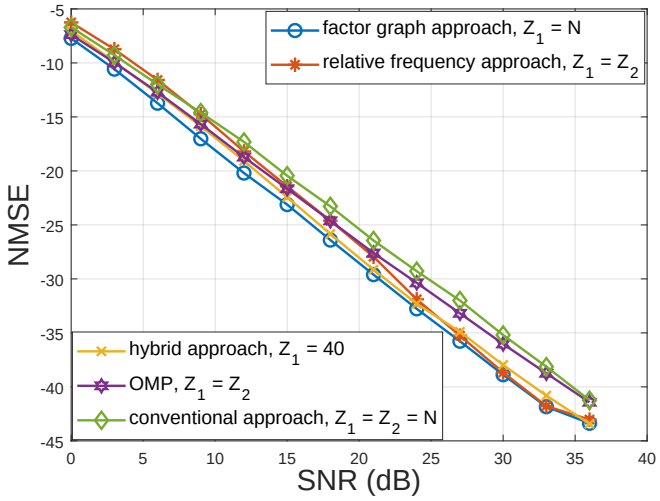

Fig. 12. NMSE of different approaches with $N = 500$, $K = 5$, $\delta = \frac{2}{5}$, $Z_2 = 8$ and $K_s = 4$.

factor graph based approaches. Since reducing the communication cost is attractive in WSN systems, we recommend the hybrid approach, which combines the communication cost advantage of the relative frequency based approach, with the performance advantage of the proposed factor graph based approach. However, in practice, we should be mindful of the requirement of the different scenarios when selecting the most suitable approach. If the reconstructed signal quality is the only requirement, then the relative frequency based approach is a good choice. By contrast, if support identification is the target, then the proposed factor graph based approach becomes the best choice. Hence, the best choice for different scenarios is different.

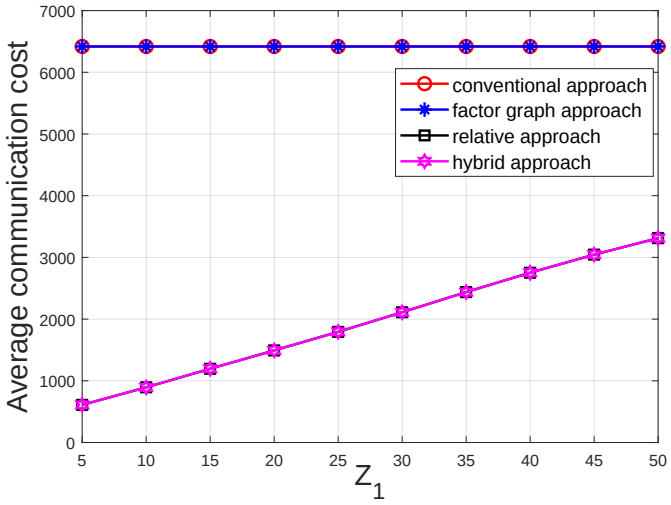

Fig. 13. The average communication cost of different approaches at $N = 500$, $K = 5$, $\delta = \frac{2}{5}$, $K_s = 4$ and SNR= 24 dB.

VI. Conclusions

Support identification is an attractive performance-boosting technique in CS-based WSN systems. This paper has intro-

duced a new technique of performing support identification, where sparse sensing matrices are employed that can satisfy the RIP1 condition of [43] for ensuring that the signal can be recovered after being compressed. In our proposed approach, we exploit support identification and the sparse nature of the sensing matrix in order to eliminate those sensor measurements that only capture noise, but do not provide useful information for signal reconstruction. We adopt factor graphs, Bayesian inference, the MAP algorithm and belief propagation to estimate the locations of non-zero entries in the sparse signal. Our results show that the proposed factor graph based approach succeeds in achieving higher support identification accuracy than the state-of-the-art relative frequency based approach and OMP algorithm, despite adopting a smaller number of measurements. Furthermore, our signal reconstruction results show that the proposed factor graph based approach has about 4 dB SNR gain over the conventional approach, in the case where the signal reconstruction NMSE is reduced to -40 dB. A hybrid approach has also been proposed for reliable support identification, which achieves a similar NMSE performance as the proposed factor graph based approach, while also achieving matching the significantly reduced communication cost of the proposed factor graph based approach, hence achieving 'the best of both worlds'. In our future work, we will consider the case where the sparsity level K jointly and is not known in advance, and in particular, we will devise techniques that can jointly and iteratively perform K estimation, support identification, and signal reconstruction.

REFERENCES

[1] D. L. Donoho, "Compressed sensing," *IEEE Trans. Inf. Theor.*, vol. 52, no. 4, pp. 1289–1306, Apr. 2006. [Online]. Available: https://doi.org/10.1109/TIT.2006.871582

[2] M. Abo-Zahhad, A. Hussein, and A. Mohamed, "Compressive sensing algorithms for signal processing applications: A survey," *International Journal of Communications, Network and System Sciences*, vol. 08, pp. 197–216, Jan. 2015.

[3] J. W. Choi, B. Shim, Y. Ding, B. Rao, and D. I. Kim, "Compressed sensing for wireless communications: Useful tips and tricks," *IEEE Communications Surveys Tutorials*, vol. 19, no. 3, pp. 1527–1550, 2017.

[4] Z. Gao, L. Dai, C. Qi, C. Yuen, and Z. Wang, "Near-optimal signal detector based on structured compressive sensing for massive SM-MIMO," *IEEE Transactions on Vehicular Technology*, vol. 66, no. 2, pp.1860–1865, 2017.

[5] D. L. Donoho, A. Maleki, and A. Montanari, "Message-passing algorithms for compressed sensing," *Proceedings of the National Academy of Sciences*, vol. 106, no. 45, pp. 18 914–18 919, 2009. [Online]. Available: https://www.pnas.org/content/106/45/18914

[6] D. L. Donoho, A. Maleki, and A. Montanari, "Message passing algorithms for compressed sensing: I. motivation and construction," in *2010 IEEE Information Theory Workshop on Information Theory (ITW 2010, Cairo)*, 2010, pp. 1–5.

[7] M. Bayati and A. Montanari, "The dynamics of message passing on dense graphs, with applications to compressed sensing," *IEEE Transactions on Information Theory*, vol. 57, no. 2, pp. 764–785, 2011.

[8] J. Ziniel and P. Schniter, "Dynamic compressive sensing of time-varying signals via approximate message passing," *IEEE Transactions on Signal Processing*, vol. 61, no. 21, pp. 5270–5284, 2013.

[9] T. T. Cai and L. Wang, "Orthogonal matching pursuit for sparse signal recovery with noise," *IEEE Transactions on Information Theory*, vol. 57, no. 7, pp. 4680–4688, 2011.

[10] A. Salim, W. Osamy, A. M. Khedr, A. Aziz, and M. Abdel-Mageed, "A secure data gathering scheme based on properties of primes and compressive sensing for IoT-based WSNs," *IEEE Sensors Journal*, vol. 21, no. 4, pp. 5553–5571, 2021.

[11] N. Lee, "MAP support detection for greedy sparse signal recovery algorithms in compressive sensing," *IEEE Transactions on Signal Processing*, vol. 64, no. 19, pp. 4987–4999, 2016.

[12] J. Chae and S. Hong, "Greedy algorithms for sparse and positive signal recovery based on bit-wise MAP detection," *IEEE Transactions on Signal Processing*, vol. 68, pp. 4017–4029, 2020.

[13] W. Chen and C. Lu, "Recovery guarantee of sparse binary sensing matrices under greedy algorithm," in *2018 International Symposium on Information Theory and Its Applications (ISITA)*, 2018, pp. 423–426.

[14] J. Jiang, H. Sun, D. Baglee, and H.V. Poor, "Achieving autonomous compressive spectrum sensing for cognitive radios," *IEEE Transactions on Vehicular Technology*, vol. 65, no. 3, pp. 1281–1291, 2016.

[15] T. Xiong, H. Li, P. Qi, Z. Li, and S. Zheng, "Predecision for wideband spectrum sensing with sub-Nyquist sampling," *IEEE Transactions on Vehicular Technology*, vol. 66, no. 8, pp. 6908–6920, 2017.

[16] P. Qi, Z. Li, H. Li, and T. Xiong, "Blind sub-Nyquist spectrum sensing with modulated wideband converter," *IEEE Transactions on Vehicular Technology*, vol. 67, no. 5, pp. 4278–4288, 2018.

[17] W. Xu, S. Wang, S. Yan, and J. He, "An efficient wideband spectrum sensing algorithm for unmanned aerial vehicle communication networks," *IEEE Internet of Things Journal*, vol. 6, no. 2, pp. 1768–1780, 2019.

[18] D. Cohen and Y. C. Eldar, "Sub-Nyquist sampling for power spectrum sensing in cognitive radios: A unified approach," *IEEE Transactions on Signal Processing*, vol. 62, no. 15, pp. 3897–3910, 2014.

[19] B. Wang, L. Dai, T. Mir, and Z. Wang, "Joint user activity and data detection based on structured compressive sensing for NOMA," *IEEE Communications Letters*, vol. 20, no. 7, pp. 1473–1476, 2016.

[20] B. K. Jeong, B. Shim, and K. B. Lee, "MAP-based active user and data detection for massive machine-type communications," *IEEE Transactions on Vehicular Technology*, vol. 67, no. 9, pp. 8481–8494, 2018.

[21] G. Lim, H. Ji, and B. Shim, "Hybrid active user detection for massive machine-type communications in IoT," in *2018 International Conference on Information and Communication Technology Convergence (ICTC)*, 2018, pp. 1049–1052.

[22] J. Ahn, B. Shim, and K. B. Lee, "EP-based joint active user detection and channel estimation for massive machine-type communications," *IEEE Transactions on Communications*, vol. 67, no. 7, pp. 5178–5189, 2019.

[23] K. Yu, Y. D. Zhang, M. Bao, Y. Hu, and Z. Wang, "DOA estimation from one-bit compressed array data via joint sparse representation," *IEEE Signal Processing Letters*, vol. 23, no. 9, pp. 1279–1283, 2016.

[24] X. Hu, N. Tong, Y. Guo, and S. Ding, "MIMO radar 3-d imaging based on multi-dimensional sparse recovery and signal support prior information," *IEEE Sensors Journal*, vol. 18, no. 8, pp. 3152–3162, 2018.

[25] T. Wimalajeewa and P. K. Varshney, "Cooperative sparsity pattern recovery in distributed networks via distributed-OMP," in *2013 IEEE International Conference on Acoustics, Speech and Signal Processing*, May 2013, pp. 5288–5292.

[26] D. Malioutov, M. Cetin, and A. S. Willsky, "A sparse signal reconstruction perspective for source localization with sensor arrays," *IEEE Transactions on Signal Processing*, vol. 53, no. 8, pp. 3010–3022, Aug. 2005.

[27] H. Liu, B. Yang, and C. Pang, "Multiple sound source localization based on TDOA clustering and multi-path matching pursuit," in *2017 IEEE International Conference on Acoustics, Speech and Signal Processing (ICASSP)*, Mar. 2017, pp. 3241–3245.

[28] E. G. Larsson and Y. Selen, "Linear regression with a sparse parameter vector," *IEEE Transactions on Signal Processing*, vol. 55, no. 2, pp. 451–460, Feb. 2007.

[29] A. Miller, *Subset Selection in Regression*, ser. Chapman & Hall/CRC Monographs on Statistics & Applied Probability. CRC Press, 2002. [Online]. Available: https://books.google.co.uk/books?id=7p59iir822sC

[30] W. Chen and I. J. Wassell, "Cost-aware activity scheduling for compressive sleeping wireless sensor networks," *IEEE Transactions on Signal Processing*, vol. 64, no. 9, pp. 2314–2323, May 2016.

[31] T. Wimalajeewa and P. K. Varshney, "Sparse signal detection with compressive measurements via partial support set estimation," *IEEE Transactions on Signal and Information Processing over Networks*, vol. 3, no. 1, pp. 46–60, March 2017.

[32] M. Yang, J. Wu, T. Wang, R. G. Maunder, and R. Gau, "Fusion-based cooperative support identification for compressive networked sensing," *IEEE Wireless Communications Letters*, vol. 9, no. 2, pp. 157–161, 2020.

[33] Z. Gao, L. Dai, S. Han, C.L. I, Z. Wang, and L. Hanzo, "Compressive sensing techniques for next-generation wireless communications," *IEEE Wireless Communications*, vol. 25, no. 3, pp. 144–153, Jun. 2018.

[34] X. Li, D. Yin, S. Pawar, R. Pedarsani, and K. Ramchandran, "Sublinear time support recovery for compressed sensing using sparse-graph

codes," *IEEE Transactions on Information Theory*, vol. 65, no. 10, pp. 6580–6619, 2019.

[35] M. Lotfi and M. Vidyasagar, "A fast noniterative algorithm for compressive sensing using binary measurement matrices," *IEEE Transactions on Signal Processing*, vol. 66, no. 15, pp. 4079–4089, 2018.

[36] L. Zhang, L. Huang, B. Li, J. Yin, and W. Bao, "Sensing matrix design for MMV compressive sensing: An MVDR approach," *IEEE Transactions on Vehicular Technology*, vol. 68, no. 9, pp. 8601–8612, 2019.

[37] X. Li, X. Tao, and Z. Chen, "Spatio-temporal compressive sensing-based data gathering in wireless sensor networks," *IEEE Wireless Communications Letters*, vol. 7, no. 2, pp. 198–201, 2018.

[38] Y. Shen, W. Hu, R. Rana, and C. T. Chou, "Nonuniform compressive sensing for heterogeneous wireless sensor networks," *IEEE Sensors Journal*, vol. 13, no. 6, pp. 2120–2128, 2013.

[39] N. Jain, V. A. Bohara, and A. Gupta, "iDEG: Integrated data and energy gathering framework for practical wireless sensor networks using compressive sensing," *IEEE Sensors Journal*, vol. 19, no. 3, pp. 1040–1051, 2019.

[40] J. Zhang, Z. Yu, L. Cen, Z. Gu, Z. Lin, and Y. Li, "Deterministic construction of sparse binary matrices via incremental integer optimization," *Inf. Sci.*, vol. 430, pp. 504–518, 2018.

[41] Z. Zhang, T. Jung, S. Makeig, and B. D. Rao, "Compressed sensing for energy-efficient wireless telemonitoring of noninvasive fetal ecg via block sparse bayesian learning," *IEEE Transactions on Biomedical Engineering*, vol. 60, no. 2, pp. 300–309, 2013.

[42] S. Li, L. D. Xu, and X. Wang, "Compressed sensing signal and data acquisition in wireless sensor networks and Internet of Things," *IEEE Transactions on Industrial Informatics*, vol. 9, no. 4, pp. 2177–2186, Nov. 2013.

[43] R. Berinde, A. C. Gilbert, P. Indyk, H. Karloff, and M. J. Strauss, "Combining geometry and combinatorics: A unified approach to sparse signal recovery," in *2008 46th Annual Allerton Conference on Communication, Control, and Computing*, Sep. 2008, pp. 798–805.

[44] G. Quer, R. Masiero, G. Pillonetto, M. Rossi, and M. Zorzi, "Sensing, compression, and recovery for wsns: Sparse signal modeling and monitoring framework," *IEEE Transactions on Wireless Communications*, vol. 11, no. 10, pp. 3447–3461, 2012.

[45] C. Karakus, A. C. Gurbuz, and B. Tavli, "Analysis of energy efficiency of compressive sensing in wireless sensor networks," *IEEE Sensors Journal*, vol. 13, no. 5, pp. 1999–2008, 2013.

[46] C. Chen and J. Wu, "Amplitude-aided 1-bit compressive sensing over noisy wireless sensor networks," *IEEE Wireless Communications Letters*, vol. 4, no. 5, pp. 473–476, 2015.

[47] M. A. Al-Jarrah, M. A. Yaseen, and A. Al-Dweik, "Decision fusion for clustered wsns over iot infrastructure using 1-bit quantization," in *2019 International Conference on Electrical and Computing Technologies and Applications (ICECTA)*, 2019, pp. 1–5.

[48] W. Li and H. Dai, "Distributed detection in wireless sensor networks using a multiple access channel," *IEEE Transactions on Signal Processing*, vol. 55, no. 3, pp. 822–833, 2007.

[49] R. Ward, "Compressed sensing with cross validation," *IEEE Transactions on Information Theory*, vol. 55, no. 12, pp. 5773–5782, Dec. 2009.

[50] D. Baron, S. Sarvotham, and R. G. Baraniuk, "Bayesian compressive sensing via belief propagation," *IEEE Transactions on Signal Processing*, vol. 58, no. 1, pp. 269–280, Jan. 2010.

[51] A. Gilbert and P. Indyk, "Sparse recovery using sparse matrices," *Proceedings of the IEEE*, vol. 98, no. 6, pp. 937–947, Jun. 2010.

[52] S. Jafarpour, W. Xu, B. Hassibi, and R. Calderbank, "Efficient and robust compressed sensing using optimized expander graphs," *IEEE Transactions on Information Theory*, vol. 55, no. 9, pp. 4299–4308, Sep. 2009.

[53] "Physical layer procedures for data (Release 15)," November 2017. [Online]. Available: https://portal.3gpp.org/ngppapp/CreateTdoc.aspx?mode=view\&contributionId=840513

[54] L. Bahl, J. Cocke, F. Jelinek, and J. Raviv, "Optimal decoding of linear codes for minimizing symbol error rate (corresp.)," *IEEE Transactions on Information Theory*, vol. 20, no. 2, pp. 284–287, Mar. 1974.

[55] J. Zhang, Z. L. Yu, Z. Gu, Y. Li, and Z. Lin, "Multichannel electrocardiogram reconstruction in wireless body sensor networks through weighted $\ell_{1,2}$ minimization," *IEEE Transactions on Instrumentation and Measurement*, vol. 67, no. 9, pp. 2024–2034, 2018.

[56] J. Koshy, I. Wirjawan, R. Pandey, and Y. Ramin, "Balancing computation and communication costs: The case for hybrid execution in sensor networks," *Ad Hoc Networks*, vol. 6, no. 8, pp. 1185–1200, 2008. [Online]. Available: https://doi.org/10.1016/j.adhoc.2007.11.006

[57] M. P. Friedlander, H. Mansour, R. Saab, and . Yilmaz, "Recovering compressively sampled signals using partial support information," *IEEE Transactions on Information Theory*, vol. 58, no. 2, pp. 1122–1134, Feb 2012.